

Hydrodynamic dispersion of pressure-induced and electroosmotic flow in porous glasses probed by Nuclear Magnetic Resonance

Yujie Li, German Farrherr, Rainer Kimmich

Universität Ulm, Sektion Kernresonanzspektroskopie, Albert-Einstein-Allee 11,
D-89069 Ulm, Germany

Corresponding author:

Yujie Li

Sektion Kernresonanzspektroskopie

Universität Ulm

Albert-Einstein-Allee 11

D-89069 Ulm, Germany

E-Mail: yujie.li@uni-ulm.de

Abstract

Fluid transport by flow in random porous media is subject to hydrodynamic dispersion. In a series of pulsed field-gradient NMR experiments, we have compared flow induced by pressure gradients on the one hand and by electroosmosis on the other. The media were porous glasses with pore dimensions from 1 to 100 μm . With increasing flow rates, a crossover from subdiffusive to superdiffusive mean-squared displacement laws was observed in both cases. This demonstrates the competition between molecular diffusion and convection, and is a typical example of anomalous transport.

1. Introduction

The theory of anomalous diffusion is well established. Propagator formalisms have been reported both for sub- and superdiffusive mean-squared displacement laws [1]. Brownian diffusion in random pore networks is subject to a subdiffusive anomaly in the so-called scaling window of the root mean-squared displacement, $a < \sqrt{\langle Z^2 \rangle} < \xi$, where a is the pore dimension and ξ is the correlation length of the pore network [2].

Hydrodynamic dispersion of fluids in porous media is a combined effect of Brownian diffusion and advection. Three mechanisms may lead to dispersion [3]: (a) Taylor dispersion caused by Brownian diffusion of fluid particles across velocity shear; (b) mechanical dispersion, an effect of advection along tortuous paths and streamline bifurcation; and (c) holdup of fluid particles in the dead ends of pore networks.

In the long time and large displacement limit [4], the propagator of the molecule (or tracer) displacements is expected to be Gaussian [5] and the mean-squared displacement $\langle Z^2 \rangle$ grows linearly in time t , i.e. $\langle Z^2 \rangle \propto t$. On the other hand, for length scales within the scaling window, particle transport is subject to anomalous laws [4]. The propagator is then non-Gaussian, and there is a tendency to power laws of the form $\langle Z^2 \rangle \propto t^\alpha$ where $\alpha \neq 1$. If $0 < \alpha < 1$, transport is called “subdiffusive” while $\alpha > 1$ indicates “superdiffusive” displacement behavior [1].

In the present study, hydrodynamic dispersion effects in disordered porous media in the presence of both pressure-induced and electroosmotic flows were examined and compared with the aid of pulsed gradient spin echo Nuclear Magnetic Resonance (PGSE-NMR) techniques [6].

2. Experiments

2.1 Samples and experimental setup

Disordered porous samples were prepared of VitraPor glasses #1, #C, #4, and #5 with nominal pore sizes of 100...160 μm , 40...60 μm , 10...16 μm and 1...1.6 μm . Figure 1 shows typical scanning electron micrographs (SEM) recorded with a Zeiss DSM 962 scanning electron microscope. The samples used for the dispersion experiments had a cylindrical shape with a diameter of 6 mm and a length of 40 mm. They were contained in PCTFE (PolyChloroTriFluoroEthylene) sample holders. In order to avoid any bypassing of the water, the sample holders were thermally shrunk on the sample cylinders by heating them first to 197°C for about 20 min. While being cold, the sample could be dropped into the sample holder. After thermal equilibration, it was tightly embraced by the PCTFE cylinder and could then no longer be removed without mechanically damaging the container.

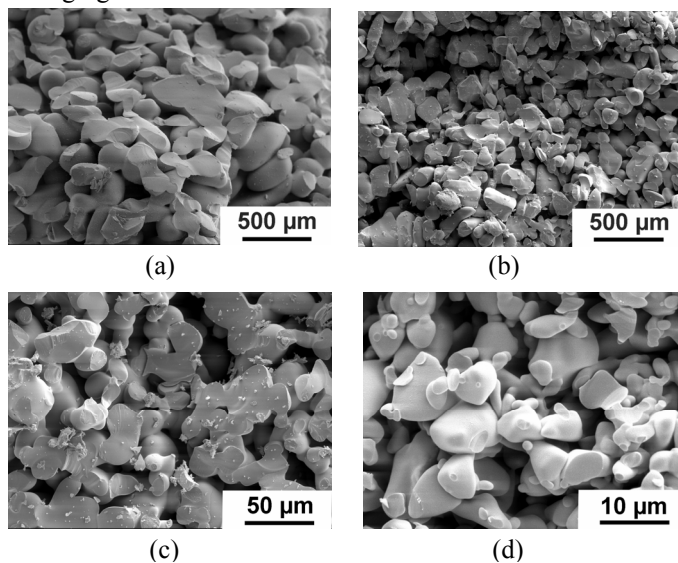


Fig. 1 Typical SEM images of (a) VitraPor #1, (b) VitraPor #C, (c) VitraPor #4, and (d) VitraPor #5 samples with nominal pore sizes of 100...160 μm , 40...60 μm , 10...16 μm and 1...1.6 μm , respectively.

Pressure-induced flow (PIF) was produced at constant flow rates of 0.1...0.9 ml/min by pumping degassed distilled water at room temperature. The flow rates can be varied in steps of 0.1 ml/min. The experimental setup is shown schematically in Fig. 2 (a). The arrows indicate the flow direction.

Electroosmotic flow (EOF) is a transport phenomenon induced by applying an electric field on a liquid electrolyte solution in channels with polar walls. Problems arising

because of Joule heating [7], [8] and effects of the oxidation and reduction processes on the electrode surfaces [8], must be carefully taken into account. U-shape design [8] of the

electrolyte cell avoids trapping of gas bubbles at the electrodes. The geometry of the Pt electrodes was designed to produce a uniform electrical field through the sample, and to permit gas to escape easily. The electrodes were wound of 1 mm thick Pt wires. Eddy current effects were therefore negligible. A Pt100 thermo resist was embedded in the sample to measure the sample temperature *in situ*. A schematic cross section of the experimental setup is shown in Fig. 2 (b). Adjustment of the position of both electrode ends and the diameters of different parts of the U-shape passage with respect to the active volume of the RF coil were thoroughly tested to minimize gas production and to eliminate signals from the bulk solution.

Electroosmotic flow was measured for voltages in the range 300...900V. The

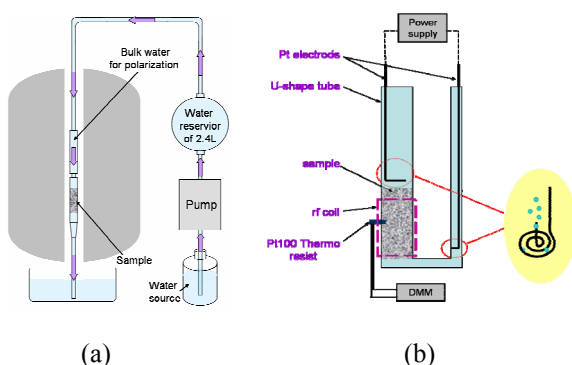


Fig. 2 Schematic figures of the experimental setups for (a) PIF and (b) EOF. The inset of (b) shows the geometry of the electrodes.

VitraPor samples were saturated with 1mM NaCl aqueous solutions. The conductivity of the bulk solution was determined with a HANNA Instruments HI 8633 conductivity meter as $1.22-1.25 \times 10^{-4} \text{ Sm}^{-1}$ at room temperature. The path length between the two electrodes was approximately 9 cm. The sample temperature was carefully controlled to be constant within 22.1...22.3°C so that Joule heating did not affect the results.

All experiments were performed with a Bruker DSX 400 NMR spectrometer equipped with a vertical 9.4 T magnet. The room temperature bore is 89 mm. A commercial Bruker gradient system with a maximum gradient strength of 1.0 T/m was employed. The PGSE-NMR technique was applied with a velocity-compensated pulse sequence to measure the effective dispersion coefficient as a function of the effective dispersion time.

2.2 Pulsed gradient NMR measuring technique with compensation of coherent velocity effects

The instantaneous velocity field \vec{v} can be analyzed in two terms according to [3]

$$\vec{v}(t) = \bar{\vec{v}} + \vec{u}(t) \quad (1)$$

where $\bar{\vec{v}} \equiv \lim_{t \rightarrow \infty} \langle \vec{v} \rangle$ is the average velocity, and $\vec{u}(t)$ is the fluctuation of the Lagrangian velocity. The principle of the NMR echo attenuation pulse sequences employed in this study is to compensate the phase shift produced by $\bar{\vec{v}}$ and to examine the echo attenuation due to $\vec{u}(t)$ [6], [9]. Since all position and velocity symbols to be used in this context refer to components along the gradient direction, we will omit the vector symbols in the following for simplicity.

The trajectory of a nucleus may be expressed as

$$r(t) = r_0 + \int_0^t v(t)dt = r_0 + \int_0^t [V + u(t)]dt = r_0 + Vt + \int_0^t u(t)dt \quad (2)$$

where r_0 is the initial position. A field gradient pulse of an arbitrary shape,

$$G = \begin{cases} G(t) & \text{for } 0 \leq t \leq T \\ 0 & \text{otherwise} \end{cases} \quad (3)$$

produces the accumulative phase shift

$$\begin{aligned} \phi(T) &= \gamma \int_0^T G(t)r(t)dt \\ &= \gamma \left[r_0 \int_0^T G(t)dt + V \int_0^T G(t)t dt + \int_0^T G(t) \int_0^t u(t')dt'dt \right] \\ &= \phi_0(T) + \phi_1(T) + \phi_2(T) \end{aligned} \quad (4)$$

where γ is the gyromagnetic ratio. The phase shifts by the position dependent term $\phi_0(T)$ and the coherent-velocity dependent term $\phi_1(T)$ can be compensated by using a bipolar gradient pulse of the form [6]:

$$G_z(t) = \begin{cases} G_0 & \text{for } 0 \leq t \leq \tau \\ -G_0 & \text{for } \tau \leq t \leq 3\tau \\ G_0 & \text{for } 3\tau \leq t \leq 4\tau \\ 0 & \text{otherwise} \end{cases} \quad (5)$$

That is, $\phi_0(T)=0$ as well as $\phi_1(T)=0$ after this bipolar gradient pulse. Merely the

fluctuation term $\phi_2(4\tau) = \gamma G \left[\int_0^T u(t)dt - \int_\tau^{3\tau} u(t)dt + \int_{3\tau}^{4\tau} u(t)dt \right]$ still contributes.

Practically, a combination of 180° radio frequency (RF) pulses and unipolar gradient pulses can be used instead of a bipolar scheme. For technical reasons, the 180° pulses can be further split into two 90° pulses each, and the gradient pulses can be composed of identical pulses of unit length δ . It ensures that the gradient amplifier produces pulses of well defined “area” $G\delta$. Fig. 3 (a) shows such a pulse sequence. Note that a combination of two 90° RF pulses effectively inverts the effect of the gradient pulses with respect to the sign. The spoiling gradient pulse spoils all spin coherences in the interval Δ . The use of 90° pulse pairs instead of 180° pulses reduces the echo amplitude by a factor of 1/4 on the one hand, but avoids excessive transverse relaxation losses on the other. The dispersion time effective for this pulse sequence is given by the combined interval 2Δ .

With tortuous flow through a porous medium, the question whether the velocity of a particle is constant depends on the length of the displacement sensitive interval. In the limit of small measuring intervals, that is, for root mean-squared displacements shorter

than the elementary length scale a , $\sqrt{\langle Z^2 \rangle} < a$, flow is not hindered and velocities tend to be constant so that the incoherent displacement contribution can only arise from Brownian diffusion.

Intervals permitting displacements in the range $a < \sqrt{\langle Z^2 \rangle} < \xi$ are connected with more or less random velocity changes so that the compensation for flow becomes incomplete. In this case, random phase shifts by tortuous flow lead to the attenuation of the echo amplitude indicating incoherent displacements. The influence of such motions will be the larger the longer the sensitive interval is, that is, the more randomly the particle trajectories develop.

Finally, for displacements $\sqrt{\langle Z^2 \rangle} > \xi$ in the sensitive interval, we have a superposition of a constant drift velocity and randomized displacements due to the tortuosity of the percolation cluster. In coherent-velocity compensation experiments, the drift contribution can completely be eliminated so that attenuation by incoherent tortuous flow governs the echo amplitude.

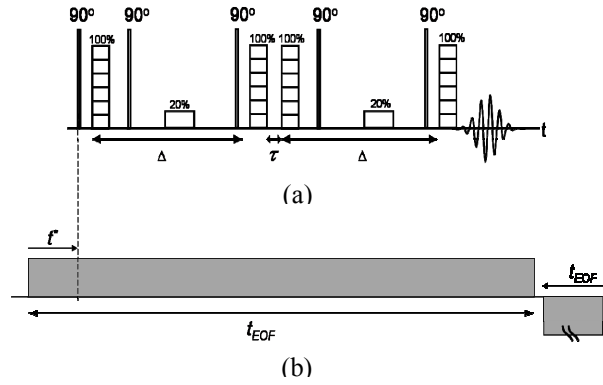


Fig. 3 (a) Coherent velocity compensated RF and field gradient pulse sequences practically used for NMR experiments probing both PIF and EOF. (b) Electrical field pulses applied to the samples during measurements for EOF.

2.3 Electrical field pulses applied during measurements of EOF

During each measurement of EOF, a pair of voltage pulses generated by a KEPCO BOP 200-1M power supply and controlled by a home built electronic device was applied to the Pt electrodes. An electrical field pulse pair as shown in Fig. 3 (b) was produced over the samples. The first pulse must be turned on with a long enough time delay t^* to achieve steady-state conditions before the corresponding phase-encoding

NMR pulse sequences starts. Experimentally, for all kinds of samples used t^* was varied from 50 ms to 150 ms. Each decay curve measured at $t^*=50$ ms and $t^* \gg 50$ ms with the other parameters kept constant agreed quite well, which indicated that EOF was fully established at the beginning of the RF pulse sequence after 50 ms. Typical echo decay curves measured at $t^*=50$ ms and $t^*=150$ ms for a VitraPor #1 sample with the largest pore size (nominally 100...160 μm) at effective dispersion times of 220 ms and voltages of 300V and 900V are compared in Fig. 4.

Uni-polar electric field pulses caused excessive gas production and chemical reactions on the surfaces of electrodes which may lead to artefacts in the measurements: (1) asymmetric anode and cathode reactions may cause a displacement of the whole water

column in the U-shaped sample tube and change the concentration of the solution; and (2) with uni-directional flow, gas produced on the anode can have much more chances to get inside the samples instead of escaping from the upper part of the U-shaped tube. Therefore a second electrical field pulse of identical length but opposite polarity was applied in each measurement cycle.

Time intervals between the two pulses in each cycle and between the cycles were set to be long enough for dissipating the Joule heating effect. In this way, the sample temperature measured in situ was kept constant. Also, long enough intervals permitted any gas bubbles to escape.

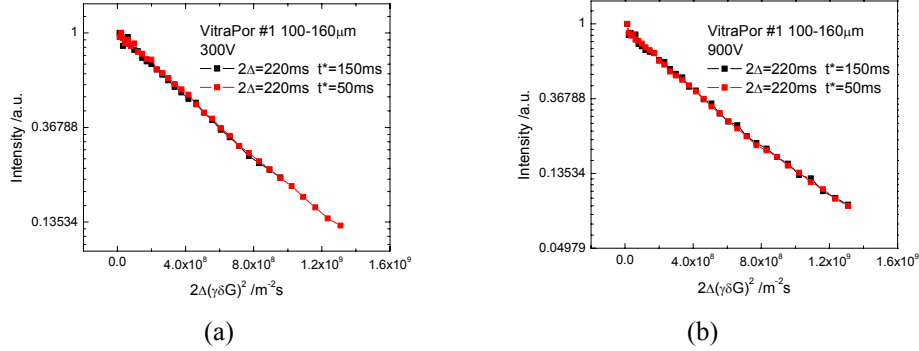


Fig. 4 Typical echo decay curves measured at $t^*=50$ ms and $t^*=150$ ms for a VitraPor #1 sample at voltages of (a) 300V and (b) 900V.

3. Results

In the limit $\sqrt{\langle Z^2 \rangle} < a$, the dispersion coefficient approaches the ordinary Brownian diffusion coefficient,

$$D_{disp} \approx D_{Brown} = const. \quad (6)$$

For $\sqrt{\langle Z^2 \rangle} \gg \xi$, the dispersion coefficient is again stationary and adopts a value,

$$D_{disp} \approx const \gg D_{Brown}. \quad (7)$$

However, in the scaling window $a < \sqrt{\langle Z^2 \rangle} < \xi$, a time dependent diffusion coefficient is expected for flow through random media at large Péclet numbers, $Pe \gg 1$,

$$D_{disp} = D_{disp}(t) \propto t^f \text{ with } 0 < f < 1 \text{ and } D_{Brown} < D_{disp}(t) < D_{eff}. \quad (8)$$

The spin echo attenuation curves measured in fluids in porous media tend to be non-exponential. For an evaluation, one therefore uses the proportionality for the low-wave-number limit,

$$E(q, t)_{q \rightarrow 0} \propto \exp(-q^2 D_{eff} t), \quad (9)$$

typical for diffusive echo attenuation experiments under ordinary conditions as an approach [10]. The wave-number is defined by $q = \gamma\delta G$ for a gradient pulse width δ . The coefficient determined in this way will be called “effective dispersion coefficient”, D_{eff} , and tends to be a function of the dispersion time, $t=2\Delta$. Furthermore anticipating that the displacement propagator can be approached by a Gaussian function, the mean-squared displacement along the gradient direction can be determined according to

$$\langle Z^2 \rangle \approx 2D_{eff}(t)t. \quad (10)$$

3.1 Hydrodynamic dispersion in PIF

For pressure-induced flow, the actual flow rates were controlled by a pump. Figure 5 (a) and (c) shows typical plots of $\langle Z^2 \rangle$ obtained for VitraPor #1 and VitraPor #C samples at different flow rates as a function of the dispersion time 2Δ [11]. A power law of the form

$$\langle Z^2 \rangle \propto (2\Delta)^\alpha \quad (11)$$

can be stated in the frame of the experimental accuracy for low and high flow rates. This applies in particular to the flow rates 0, 0.7- 0.9 ml/min. Obviously, a crossover between the subdiffusive limit in the absence of flow to a superdiffusive limit in the presence of strong enough flow occurs. The fitted exponents are $\alpha \approx 0.84$ and $\alpha \approx 1.95$, respectively, for the time window probed in the experiments.

The root mean-squared displacements evaluated from the experiments ranges from 10 to 200 μm . This is the length scale of the pore space topology of the examined porous glass. That is, the transport properties refer to the scaling window where a power law behavior can be expected. In the absence of flow, transport is governed by molecular diffusion obstructed by the confining geometry. The consequence is a subdiffusive mean-squared displacement law. Above a flow rate of about 0.7 ml/min, the exponent $\alpha \approx 1.95$ indicates a super-diffusive law even approaching the “ballistic” case $\alpha=2$. In this limit, particles are displaced in all directions with the same mean velocity. For hydrodynamic dispersion in disordered porous media, this is the case when pure mechanical mixing under the influence of the local geometry is relevant as demonstrated with computer simulations by Duplay and Sen [12].

The dependence of D_{eff} on the Péclet number (Pe) is also of interest. It reflects the nature of the mixing process. At Péclet numbers in the range of $5 < \text{Pe} < 300$, a law of the form

$$\frac{D_L}{D_m} = c_0 + c_L (\text{Pe})^{\beta_L} \quad (12)$$

is expected [4], where c_0 and c_L are numerical constants. The empirical value of the exponent is $\beta_L \approx 1.2$. In this regime, dispersion is dominated by convection, but the effect of molecular diffusion is not entirely negligible.

The mean flow velocity in a porous medium is given by

$$V = \frac{f_r}{A\phi\eta}, \quad (13)$$

where f_r is the flow rate, A the area of the cross section of the sample, Φ the porosity, and η the tortuosity. η is defined as D_{Is}/D_m , where D_{Is} is the effective dispersion coefficient in the saturated porous medium for $2\Delta=1$ s in the absence of flow, and D_m is the molecular diffusivity of bulk water. As usual, the Péclet number is defined as the ratio of a coherent and an incoherent transport quantity,

$$Pe = \frac{V\xi}{D_m} \quad (14)$$

The correlation length ξ is assumed to be three times the pore size. The mean velocity, V , ranges from $9.75 \times 10^{-5} \text{ ms}^{-1}$ to $1.2 \times 10^{-3} \text{ ms}^{-1}$. The Péclet number varies accordingly from 8 to 140.

Figures 5 (b) and (d) show plots of the ratio D_{eff}/D_m versus Pe determined according to Eq. (14) with the dispersion time as a parameter [11]. For comparison, the power law

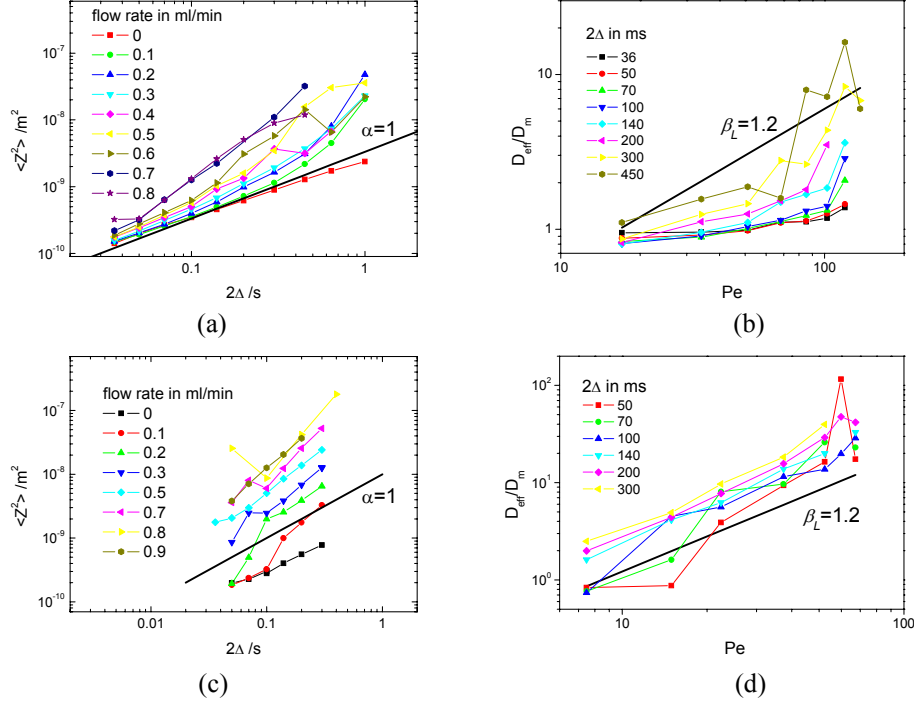


Fig. 5 Hydrodynamic dispersion for PIF. (a) and (c) Mean squared displacement, $\langle Z^2 \rangle$, as a function of the effective dispersion time, 2Δ , at different flow rates for VitraPor #1 and VitraPor #C, respectively. The bulk line represents $\langle Z^2 \rangle \sim 2\Delta$. (b) and (d) Dependence of the effective dispersion coefficient D_{eff} on the Péclet number, Pe , at different dispersion times 2Δ for VitraPor #1 and VitraPor #C. The solid straight line represents the empirical power law $D_{eff}/D_m \propto Pe^{\beta_L}$ with $\beta_L=1.2$. The thin lines between data points serve as a guide for the eye.

given in Eq. (12) is also plotted for an exponent $\beta_L=1.2$. The data in Fig. 5 (d) can be approximated by this law, but a more complicated relationship is suggested by the plot in Fig. 5(b).

3.2 Hydrodynamic dispersion in EOF

For electroosmotic flow, assuming a Boltzmann charge density distribution of the ions near the matrix surface and employing the Debye-Hückel approximation, the average velocity of EOF in a slit and/or a cylindrical microchannel is expected to be a linear function of the applied electrical field strength E_{ext} and the zeta potential ζ [7]

$$v_{av} \propto \frac{\varepsilon\varepsilon_0}{\eta} E_{ext} \zeta \quad (15)$$

ε and ε_0 are the dielectric constants in the medium and in the vacuum, respectively. η is the dynamic viscosity of the fluid. In our experiments, the voltage applied to the electrodes across the sample varied from 300 to 900V while the path length in the electrolyte solution from electrode to electrode was about 9 cm. Consequently the higher the voltage applied, the stronger the produced flow could be expected.

Fig. 6 (a), (c), and (e) show the effective dispersion coefficient D_{eff} measured as a function of the dispersion time 2Δ at different voltages for VitraPor #5, #4, and #1 samples while Fig. 6 (b), (d), and (f) display the corresponding mean-squared displacement $\langle Z^2 \rangle$ derived by Eq. (10). For VitraPor #5 with a pore size of 1-1.6 μm , D_{eff} first decreased sharply and then increased slightly with 2Δ in the presence of EOF [see Fig. 6 (a)]. Likewise, D_{eff} first decreased and then sharply increased with 2Δ in VitraPor #1 with a pore size of 100-160 μm under EOF [Fig. 6 (e)]. In both cases, a minimum value of D_{eff} could be clearly defined at a certain characteristic dispersion time between 130...170ms. Beyond this characteristic dispersion time a crossover from subdiffusive to normal or superdiffusive displacement power law behavior was identified in Fig. 6 (b) and (f) for VitraPor #5 and VitraPor #1, respectively. The dependence of D_{eff} and $\langle Z^2 \rangle$ on 2Δ [see Fig. 6 (c) and (d)] in VitraPor #4 with a medium pore size of 10-16 μm lies between the behavior observed with VitraPor #5 and #1.

For all three kinds of samples, the dispersion coefficient was enhanced as the external electrical field was increased. This can certainly be taken as an obvious indication of electroosmotic flow. Hydrodynamic dispersion became more effective when the pore size was larger. For VitraPor #1, at dispersion times longer than the characteristic value of 130 ms, the exponent α obtained by fitting Eq. (11) to the data increased from about 0.88 in the absence of electrical field to about 1.85 for the highest electrical field applied. At shorter effective dispersion times, only a subdiffusive displacement law fitted to the experimental data.

The existence of a minimum value for D_{eff} may indicate the competitive action of pore space restrictions at short times (D_{eff} decreases) and mechanical dispersion at long times (D_{eff} increases). In the inset of Fig. 6 (e), a plot of D_{eff} vs. 2Δ for a VitraPor #1 sample under pressure-induced flow is shown for comparison. A slight tendency to reach a minimum value of D_{eff} could also be found in the same range of dispersion time at a flow rate smaller than 0.3 ml/min.

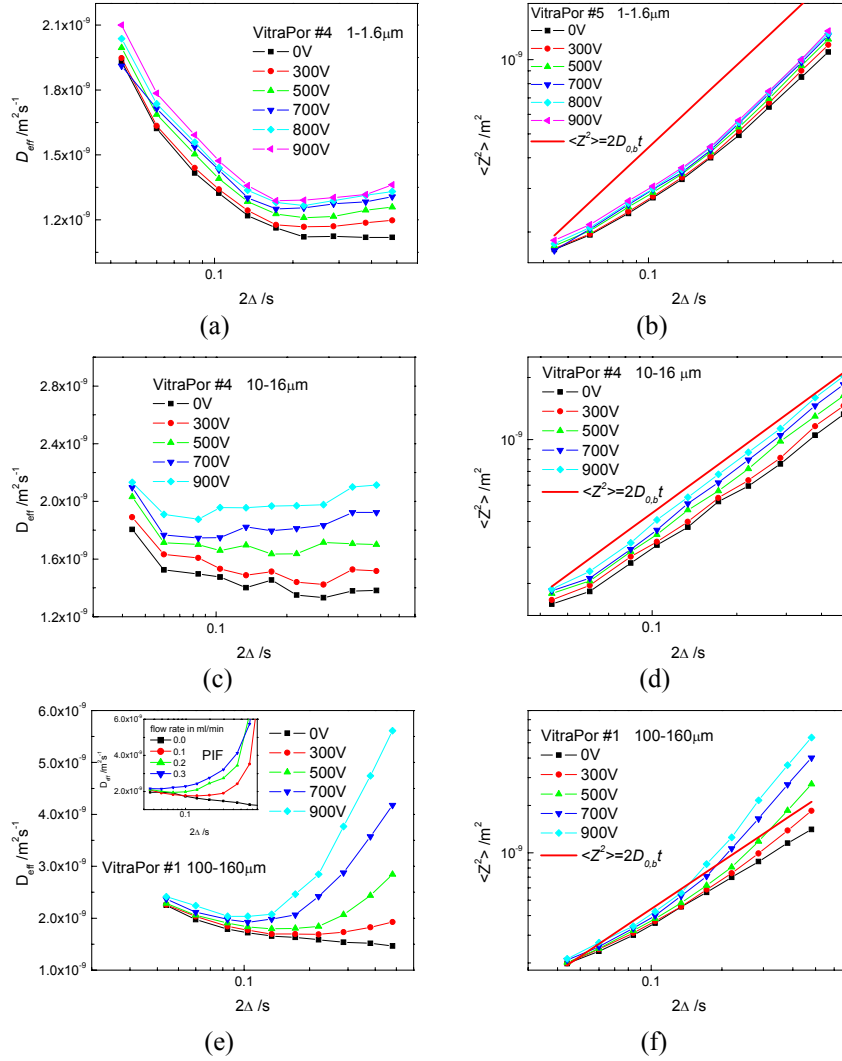


Fig. 6 Hydrodynamic dispersion for EOF. (a), (c), and (e) The effective dispersion coefficient, D_{eff} , measured as a function of the effective dispersion time, 2Δ , at different flow rates in VitraPor #5, VitraPor #4, and VitraPor #1, respectively. The inset of (e) a plot of D_{eff} vs. 2Δ for a VitraPor #1 sample under pressure-induced flow. (b), (d), and (f) Mean-squared displacement, $\langle Z^2 \rangle$, as a function of 2Δ , at different flow rates in VitraPor #5, VitraPor #4, and VitraPor #1, respectively. The solid straight line represents $\langle Z^2 \rangle = 2D_{0,b}t$, where $D_{0,b}$ stands for the diffusion coefficient in the bulk solution at zero voltage. The thin lines between data points serve as a guide for the eye.

4. Discussion and conclusions

Molecular diffusion and hydrodynamic dispersion were studied by a PFG-NMR technique in disordered porous glasses for pressure-induced and electroosmotic flows. In both cases subdiffusive behavior were found in the absence of flow while superdiffusive mean-squared displacement laws were evaluated at high flow rates/high electrical fields in the scaling window. The crossover from sub- to superdiffusive behavior as increasing the flow rates indicated the competition between molecular diffusion and convection.

In EOF, a minimum value of D_{eff} at a characteristic dispersion time can be clearly identified in comparison with PIF. The velocity distribution in the flow field for EOF and PIF is expected to be different. In the case of a two-dimensional tube with smooth surfaces, the velocity distribution with PIF should take a parabolic shape while with EOF a plug-like distribution is relevant as schematically illustrated in Fig. 7 (a) and (b). The existence of a characteristic dispersion time indicates a characteristic length scale in the pore size structure. Hydrodynamic dispersion overcomes pore space restrictions only when molecules can experience a root mean-squared displacement exceeding the characteristic length scale and this becomes visible in the EOF case due to the uniform velocity distribution.

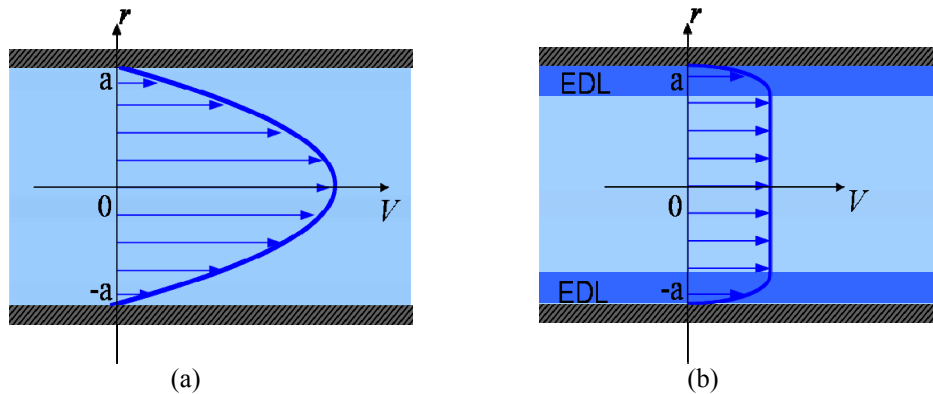


Fig. 7 Schematic flow velocity distributions for EOF and PIF in a two-dimensional tube with smooth surfaces

References

- [1] R. Metzler and J. Klafter, Phys. Reports 339(2000) 1-77.
- [2] R. Orbach, Science 814 231(1986) 814-819.
- [3] P. T. Callaghan, S. L. Codd, J. D. Seymour, Concepts in Magn. Reson., 11(4), 181 (1999).
- [4] M. Sahimi, Flow and transport in porous media and fractured rock: from classical methods to modern approaches. VCH Ltd. 1995.
- [5] U. M. Scheven and P. N. Sen, Phys. Rev. Lett. 89(25), 254501(2002).

- [6] R. Kimmich, NMR Tomography, Diffusometry, Relaxometry, Springer-Verlag, Berlin, 1997.
- [7] D. Li, Electrokinetics in Microfluidics (Elsevier Academic Press, 2004).
- [8] E. Pettersson, I. Furó, and P. Stilbs, *Concept. Mag. Res. A.*, 22A(2), 61(2004).
- [9] A. A. Khrapitchev and P. T. Callaghan, *Phys. Fluids* 15(9), 2649(2003).
- [10] R. Kimmich, *Chem. Phys.* 284, 253 (2002).
- [11] Y. Li, G. Farrher, and R. Kimmich, *Phys. Rev. E* 74(2006) 066309.
- [12] R. Duplay, and P. N. Sen, *Phys. Rev. E* 70, 066309(2004).